# Stable and unstable orbits around Mercury

Zoltán Makó, Ferenc Szenkovits, Júlia Salamon, Robert Oláh-Gál

**Celestial Mechanics and Dynamical Astronomy manuscript No.**
(will be inserted by the editor)

# Stable and Unstable Orbits around Mercury

**Zoltán Makó · Ferenc Szenkovits · Júlia Salamon · Robert Oláh-Gál**

Received: date / Accepted: date

**Abstract** This paper provides a study of the stable and unstable regions around the smaller primary in the framework of the spatial elliptic restricted three-body problem. The definitions and methods used to determine stable and unstable regions are extended to three dimensions. New results concerning the stable and unstable regions around Mercury are obtained in the SunMercury system.

**Keywords** weak stability boundary · weak capture · spatial elliptic restricted three-body problem

**PACS** 95.10.Ce · 96.30.Dz · 45.10.Na

**Mathematics Subject Classification (2000)** 70F07 · 70F15 · 37N05

## 1 Introduction

The capture of small bodies by major planets is an important phenomenon in planetary systems. The phenomenon has applications to the study of comets, asteroids, irregular satellites of the giant planets and different types of low energy planetary transfers, as well. Ballistic capture (or weak capture) is analytically defined for the $n$-body problem, and it monitors the sign of the Kepler energy with respect to a massive primary. In fact,

Sapientia University, Department of Mathematics and Informatics
Miercurea Ciuc, Romania
Tel.: +40 266 314 657
Fax: +40 266 372 099
E-mail: makozoltan@sapientia.siculorum.ro

Babeş-Bolyai University, Department of Applied Mathematics
Cluj-Napoca, Romania
E-mail: fszenko@math.ubbcluj.ro

Sapientia University, Department of Mathematics and Informatics
Miercurea Ciuc, Romania
E-mail: salamonjulia@sapientia.siculorum.ro

Babeş-Bolyai University, Department of Informatics
Cluj-Napoca, Romania
E-mail: ogrogrogr@gmail.com

this is a capture where the Kepler energy of the small body is non-positive with respect to the primary and its motion is stable. Such captures are generally temporary. In the framework of the circular restricted three-body problem (CRTBP) weak capture occurs in special regions of the phase space, namely around one of the two primaries (e.g. the Moon in the case of the Earth–Moon system), which are referred to as the Weak Stability Boundaries (WSB). These regions are the boundary of the stable regions, delimiting stable and unstable orbits. WSB was first introduced in 1986 to design low energy transfers to the Moon (Belbruno and Miller 1993) and it is rigorously defined in (Belbruno 2004).

Recently, WSB transfers have been more and more often considered within the framework of the treatment of trajectories lying on a manifold-shaped surface. These transfers represent special solutions of the CRTBP (see Romagnoli and Circi 2009; Belbruno 2004). The "Space Manifold Dynamics" (SMD) is the common term for the different kinds of applications to mission design, which was proposed in (Perozzi and Ferraz-Mello 2009; García and Gómez 2007).

By using the model of the planar CRTBP, Topputo and Belbruno computed the WSB in the case of the Sun-Jupiter system (Topputo and Belbruno 2009). They compared their results with the WSB of Earth-Moon system. Nagler constructed orbit type diagrams presenting detailed information about the extent and position of bounded, unbounded, and crash orbits in the framework of the planar CRTBP (Nagler 2005).

The model of the CRTBP is not adequate if the two primaries revolve on elongated orbits. In this case the Elliptic Restricted Three-Body Problem (ERTBP), where the primaries are supposed to revolve on ellipses, gives us more realistic results. In the last years, this model has been investigated from different viewpoints. Recently, within the framework of the ERTBP, Érdi et al. have determined the size of stable regions around the Lagrangian point L4, applying numerical integrations (Érdi et al. 2009). Szenkovits and Makó gave a new method to investigate the Hill stability of extrasolar planets in stellar binary systems, by using the three dimensional ERTBP (Szenkovits and Makó 2008). The planet Mercury is a good example to illustrate why is important to use the ERTBP approximation instead of the CRTBP approximation when we investigate such a celestial system. With a value slightly larger than 0.2, the Mercury's orbital eccentricity is more than twice as big as that of any other planets in the solar system (Yeomans 2007). It follows that the computation of Mercury's WSB inevitably requires the ERTBP dynamics. Indeed, the ESAs BepiColombo mission intends to utilize solar perturbation to achieve the Mercurial capture of the spacecraft (Jehn et al. 2004). At the end of the transfer, a gravitational capture at the WSB of Mercury is planned to be performed by exploiting the gravity of the Sun (Jehn et al. 2008).

In this paper we give an algorithmic definition of the WSB in the three-dimensional case. This is a generalization of the definition given by Romagnoli and Circi in 2009. Then, by using the capture effect, we show that WSBs are subsets of the regions where the variation of the capture effect is chaotic. In the last part we investigate the properties of the stable and unstable regions in the Sun-Mercury system for different values of the orbital inclination and initial true anomaly. We use for this the spatial ERTBP.

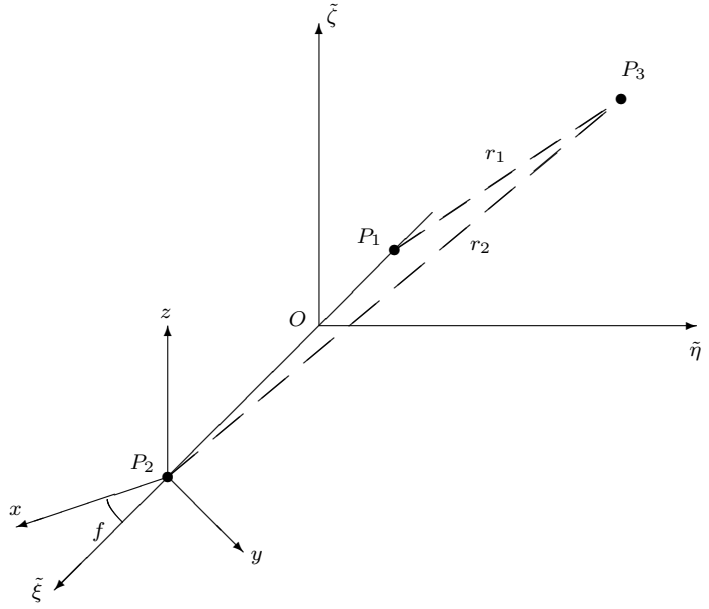


**Fig. 1** The non-rotating ($P_2xyz$) and the rotating-pulsating ($O\tilde{\xi}\tilde{\eta}\tilde{\zeta}$) frames

### 1.1 The spatial elliptic restricted three-body problem

In the ERTBP two massive primaries $P_1$ and $P_2$, with masses $m_1$ and $m_2$ revolve on elliptical orbits under their mutual gravitational attraction and the motion of a third, massless body is investigated. The variation of the mutual distance $R = \|P_1P_2\|$ with respect to the true anomaly $f$ is governed by

$$R = \frac{a\left(1-e^2\right)}{1+e\cos f}, \tag{1}$$

where $a$ and $e$ are the semimajor axis and the eccentricity of the elliptical orbit of $P_2$ around $P_1$.

To obtain a relatively simple set of equations, we use a nonuniform rotating and pulsating coordinate system (Szebehely 1967). The origin $O$ of this system is considered to be the center of mass of the two massive primaries, the $\tilde{\xi}$ axis is directed towards $P_2$, and the $\tilde{\xi}\tilde{\eta}$ coordinate-plane rotate with variable angular velocity, in such a way, that the two massive primaries are always on the $\tilde{\xi}$ axis, and the period of the rotation is $2\pi$. Besides the rotation, the system also pulsates, to keep the primaries in fixed positions ($\tilde{\xi}_1 = -\mu$, $\tilde{\eta}_1 = \tilde{\zeta}_1 = 0$, $\tilde{\xi}_2 = 1-\mu$, $\tilde{\eta}_2 = \tilde{\zeta}_2 = 0$). In this system the equations of motion of the third massless particle are:

$$\tilde{\xi}'' - 2\tilde{\eta}' = \frac{\partial\omega}{\partial\tilde{\xi}}, \qquad \tilde{\eta}'' + 2\tilde{\xi}' = \frac{\partial\omega}{\partial\tilde{\eta}}, \qquad \tilde{\zeta}'' = \frac{\partial\omega}{\partial\tilde{\zeta}}, \tag{2}$$

where the derivatives are taken with respect to the true anomaly $f$, and

$$\omega = (1 + e\cos f)^{-1}\,\Omega,$$

with

$$\Omega\left(\tilde{\xi},\tilde{\eta},\tilde{\zeta},f\right) = \frac{1}{2}\left(\tilde{\xi}^2+\tilde{\eta}^2-e\tilde{\zeta}^2\cos f\right) + \frac{1-\mu}{\sqrt{\left(\tilde{\xi}+\mu\right)^2+\tilde{\eta}^2+\tilde{\zeta}^2}} + \frac{\mu}{\sqrt{\left(\tilde{\xi}-1+\mu\right)^2+\tilde{\eta}^2+\tilde{\zeta}^2}} + \frac{1}{2}\mu\left(1-\mu\right).$$

As a generalization of the Jacobi integral existing in the planar ERTBP (Szebehely 1967), in this case we can deduce an invariant relation of the form:

$$v^2 = 2\omega - e\int_{f_0}^{f}\frac{\tilde{\zeta}^2\sin f}{1+e\cos f}df - 2e\int_{f_0}^{f}\frac{\Omega\sin f}{\left(1+e\cos f\right)^2}df - C_0, \tag{3}$$

where $v$ is the velocity of the third massless particle, with

$$v^2 = \left(\frac{d\tilde{\xi}}{df}\right)^2 + \left(\frac{d\tilde{\eta}}{df}\right)^2 + \left(\frac{d\tilde{\zeta}}{df}\right)^2.$$

For a given set of initial conditions $(\tilde{\xi}_0,\tilde{\eta}_0,\tilde{\zeta}_0,v_0,f_0)$ we have

$$C_0 = \frac{2\Omega\left(\tilde{\xi}_0,\tilde{\eta}_0,\tilde{\zeta}_0,f_0\right)}{1+e\cos f_0} - v_0^2.$$

The zero velocity surfaces (ZVS) in the ERTBP corresponding to initial conditions $(\tilde{\xi}_0,\tilde{\eta}_0,\tilde{\zeta}_0,v_0,f_0)$ are given by the equation $2\Omega\left(\tilde{\xi},\tilde{\eta},\tilde{\zeta},f\right) = C\left(f\right)$, that is

$$\left(\tilde{\xi}^2+\tilde{\eta}^2-e\tilde{\zeta}^2\cos f\right) + \frac{2\left(1-\mu\right)}{r_1} + \frac{2\mu}{r_2} + \mu\left(1-\mu\right) = C\left(f\right), \tag{4}$$

where

$$C\left(f\right) = \left(1+e\cos f\right)\left(C_0 + e\int_{f_0}^{f}\frac{\tilde{\zeta}^2\sin f}{1+e\cos f}df + 2e\int_{f_0}^{f}\frac{\Omega\sin f}{\left(1+e\cos f\right)^2}df\right), \tag{5}$$

and $r_1 = \sqrt{\left(\tilde{\xi}+\mu\right)^2+\tilde{\eta}^2+\tilde{\zeta}^2}$, $r_2 = \sqrt{\left(\tilde{\xi}-1+\mu\right)^2+\tilde{\eta}^2+\tilde{\zeta}^2}$. These surfaces delimit the Hill-regions, in which the motion of the third particle is possible.

With the variation of the true anomaly $f$, these ZVS (4) change continuously over time. They change their topological type, and size as well. This fluctuation is due to the variation of $C\left(f\right)$ and to the presence of the variable term $-e\tilde{\zeta}^2\cos f$ (see Figure 2).

As known in the case of the restricted three-body problem, for $C > C_2 = C_{cr}$, where $C_2$ corresponds to the interior collinear Lagrangian point $L_2$, ZVS have two closed ellipsoidal components around the two primaries and a third component, with variable topological type (ellipsoidal for $e\cos f < 0$, cylindric for $e\cos f = 0$ and

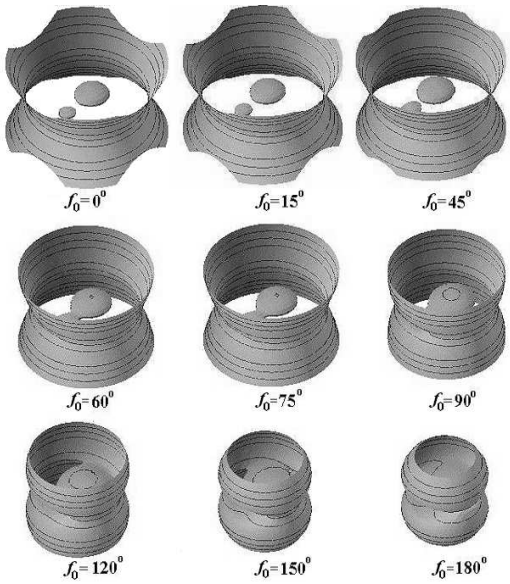


**Fig. 2** Variable ZVS in the ERTBP

hyperboloidal for $e\cos f > 0$). When $C > C_2$, $P_3$ can move either around $P_1$ or $P_2$, in the two inner regions, or around both of these bodies in the outer region, but it cannot move from one region into the other. This can occur only when there exists $f \in \mathbb{R}$ such that $C(f) \leq C_2$. When $C$ decreases, $P_3$ becomes more energetic, and the size of the region where $P_3$ can move becomes larger and larger.

In the case of the ERTBP the measure of the Hill stability of the small particle with respect to $P_2$ is

$$S(f) = \frac{C(f) - C_{cr}}{C_{cr}}. \tag{6}$$

Szenkovits and Makó proved that $S(f)$ presents local extremums for $f = k\pi$ $(k \in \mathbb{Z})$, which increase if $f \in \cup_{k\in\mathbb{Z}}[2k\pi, (2k+1)\pi]$ and decrease if $f \in \cup_{k\in\mathbb{Z}}[(2k+1)\pi, (2k+2)\pi]$ (Szenkovits and Makó 2008).

The variation of $C(f)$ correlated with the variation of $S(f)$ shows that the ZVS (4) present a rhythmical ($2\pi$ periodic) variation, a "pulsation". If the value of $C(f)$ does not cross certain critical values, these surfaces only pulsate (with variable amplitude) preserving their topological type. If the value of $C(f)$ passes through critical values, then the ZVS change their topological type (see Figure 2).

Let

$$\gamma(f) = (\tilde{\xi}(f), \tilde{\eta}(f), \tilde{\zeta}(f), \tilde{\xi}'(f), \tilde{\eta}'(f), \tilde{\zeta}'(f)),$$

or

$$\gamma(t) = (x(t), y(t), z(t), \dot{x}(t), \dot{y}(t), \dot{z}(t)),$$

$t, f \in \mathbb{R}$, denote the flows of the differential equations (2) describing the motion of $P_3$ in the model of the ERTBP.

1.2 The Kepler-energy

To investigate the capture of the test particle $P_3$ by the primary $P_2$, we need a new, "fixed" (non-rotating) system of coordinates $P_2xyz$. Positions given it these two reference frame are connected through the next equations:

$$\begin{bmatrix}\tilde{\xi}\\ \tilde{\eta}\\ \tilde{\zeta}\end{bmatrix} = \begin{bmatrix}\cos f & \sin f & 0\\ -\sin f & \cos f & 0\\ 0 & 0 & 1\end{bmatrix}\begin{bmatrix}\frac{x}{R}\\ \frac{y}{R}\\ \frac{z}{R}\end{bmatrix} + \begin{bmatrix}1-\mu\\ 0\\ 0\end{bmatrix}, \tag{7}$$

$$\begin{bmatrix}x\\ y\\ z\end{bmatrix} = R\begin{bmatrix}\cos f & -\sin f & 0\\ \sin f & \cos f & 0\\ 0 & 0 & 1\end{bmatrix}\begin{bmatrix}\tilde{\xi}-1+\mu\\ \tilde{\eta}\\ \tilde{\zeta}\end{bmatrix}. \tag{8}$$

The components of the velocities are transformed with:

$$\begin{bmatrix}\tilde{\xi}'\\ \tilde{\eta}'\\ \tilde{\zeta}'\end{bmatrix} = \frac{1}{R}\begin{bmatrix}\cos f & \sin f & 0\\ -\sin f & \cos f & 0\\ 0 & 0 & 1\end{bmatrix}\left(\frac{1}{\frac{df}{dt^*}}\begin{bmatrix}\dot{x}\\ \dot{y}\\ \dot{z}\end{bmatrix}\right. \tag{9}$$
$$\left. +\frac{a\left(1-e^2\right)}{\left(1+e\cos f\right)^2}\begin{bmatrix}-e\sin f & e\cos f+1 & 0\\ -e\cos f-1 & -e\sin f & 0\\ 0 & 0 & -e\sin f\end{bmatrix}\begin{bmatrix}\frac{x}{R}\\ \frac{y}{R}\\ \frac{z}{R}\end{bmatrix}\right)$$

$$\begin{bmatrix}\dot{x}\\ \dot{y}\\ \dot{z}\end{bmatrix} = \frac{df}{dt^*}\left(R\begin{bmatrix}\cos f & -\sin f & 0\\ \sin f & \cos f & 0\\ 0 & 0 & 1\end{bmatrix}\cdot\begin{bmatrix}\tilde{\xi}'\\ \tilde{\eta}'\\ \tilde{\zeta}'\end{bmatrix}\right. \tag{10}$$
$$\left. +\frac{a\left(1-e^2\right)}{\left(1+e\cos f\right)^2}\begin{bmatrix}-\sin f & -e-\cos f & 0\\ e+\cos f & -\sin f & 0\\ 0 & 0 & e\sin f\end{bmatrix}\cdot\begin{bmatrix}\tilde{\xi}-1+\mu\\ \tilde{\eta}\\ \tilde{\zeta}\end{bmatrix}\right),$$

where

$$\frac{df}{dt^*} = \frac{1}{\left(1-e^2\right)^{3/2}}\left(1+e\cos f\right)^2,$$

the period $P = 2\pi$, and $R$ is given in (1).

The velocity of the test particle $P_3$ with respect to the non-rotating reference frame $P_2xyz$ is

$$\begin{aligned}\dot{x}^2+\dot{y}^2+\dot{z}^2 = \frac{a^2}{1-e^2}\Big[&\left(1+e\cos f\right)^2\left(\tilde{\xi}'^2+\tilde{\eta}'^2+\tilde{\zeta}'^2\right)\\ &+\left(\left(1+e\cos f\right)^2+e^2\sin^2 f\right)\left(\left(\tilde{\xi}+\mu-1\right)^2+\tilde{\eta}^2+\tilde{\zeta}^2\right)\\ &-\left(1+e\cos f\right)^2\tilde{\zeta}^2\\ &+2e\sin f\left(1+e\cos f\right)\left(\left(\tilde{\xi}+\mu-1\right)\tilde{\xi}'+\tilde{\eta}\tilde{\eta}'+\tilde{\zeta}\tilde{\zeta}'\right)\\ &+2\left(1+e\cos f\right)^2\left(\left(\tilde{\xi}+\mu-1\right)\tilde{\eta}'-\tilde{\eta}\tilde{\xi}'\right)\Big].\end{aligned} \tag{11}$$

Let $r_2$ and $v_2$ denote the magnitude of the distance and the velocity of the massless particle $P_3$ with respect to the primary $P_2$ in the non-rotating system. The *Kepler energy* of $P_3$ with respect to $P_2$ is

$$H_2 = \frac{v_2^2}{2} - \frac{\mu}{r_2}, \tag{12}$$

where $r_2^2 = x^2 + y^2 + z^2 = R^2 \left[ \left( \tilde{\xi} + \mu - 1 \right)^2 + \tilde{\eta}^2 + \tilde{\zeta}^2 \right]$, and $v_2^2$ expressed in the $P_2$-centered non-rotating coordinates is $v_2^2 = \dot{x}^2 + \dot{y}^2 + \dot{z}^2$. In the non-rotating system we consider the normalized units $a\,(1-e) = 1$ and $\frac{2\pi}{P} = 1$. Thus, the Kepler-energy of the small particle with respect to $P_2$ is

$$\begin{aligned} H_2\left(\gamma\left(f\right)\right) = \frac{1}{2\left(1+e\right)} \Big[ & \left(1+e\cos f\right)^2 \left( \tilde{\xi}'^2 + \tilde{\eta}'^2 + \tilde{\zeta}'^2 \right) \\ & + \left( \left(1+e\cos f\right)^2 + e^2 \sin^2 f \right) \left( \left( \tilde{\xi} + \mu - 1 \right)^2 + \tilde{\eta}^2 + \tilde{\zeta}^2 \right) \\ & - \left(1+e\cos f\right)^2 \tilde{\zeta}^2 \\ & + 2e \sin f \left(1+e\cos f\right) \left( \left( \tilde{\xi} + \mu - 1 \right) \tilde{\xi}' + \tilde{\eta}\tilde{\eta}' + \tilde{\zeta}\tilde{\zeta}' \right) \\ & + 2\left(1+e\cos f\right)^2 \left( \left( \tilde{\xi} + \mu - 1 \right) \tilde{\eta}' - \tilde{\eta}\tilde{\xi}' \right) \\ & - \frac{2\mu\left(1+e\cos f\right)}{\sqrt{\left( \tilde{\xi} + \mu - 1 \right)^2 + \tilde{\eta}^2 + \tilde{\zeta}^2}} \Big] . \end{aligned}$$

## 2 Stable and unstable orbits in the spatial elliptic restricted three-body problem

The concept of the WSB was introduced by Belbruno and Miller (1993) and refined later by García and Gómez (2007), Belbruno et al. (2008), Topputo and Belbruno (2009), and Romagnoli and Circi (2009). Here we extend the definition of the WSB to three dimensions. For this, we consider trajectories of $P_3$ with the following initial conditions:

(i) For a fixed value of the true anomaly $f = f_0$ we consider the plane $\mathit{\Pi}\left(i, f\right)$ with inclination $i \in [0, 90^0]$ to the orbital plane of the primaries. The intersection of the orbital plane $\mathit{\Pi}\left(i, f\right)$ with the plane $\mathit{\Pi}\left(i, f\right)$ is the line $P_1P_2$ ($\mathit{\Pi}\left(i, f\right)$ marked light gray in Figure 3.a).

(ii) The initial position of the trajectory is on the half-line $l(\alpha, i, f)$ lying in the plane $\mathit{\Pi}\left(i, f\right)$ starting from $P_2$ and making an angle $\alpha \in [0, 360^0)$ with the $P_1P_2$ axis (Figure 3.a). The massless particle $P_3$ is assumed to start from the periapsis of an osculating ellipse around $P_2$, whose semi-major axis lies on $l(\alpha, i, f)$ and whose eccentricity $e_3$ is held fixed along $l(\alpha, i, f)$. In this case the initial distance between $P_2$ and $P_3$ relative to the $P_2xyz$ reference frame is $r_0 = a_3\left(1 - e_3\right)$, where $a_3$ is the semi-major axis of the osculating ellipse.

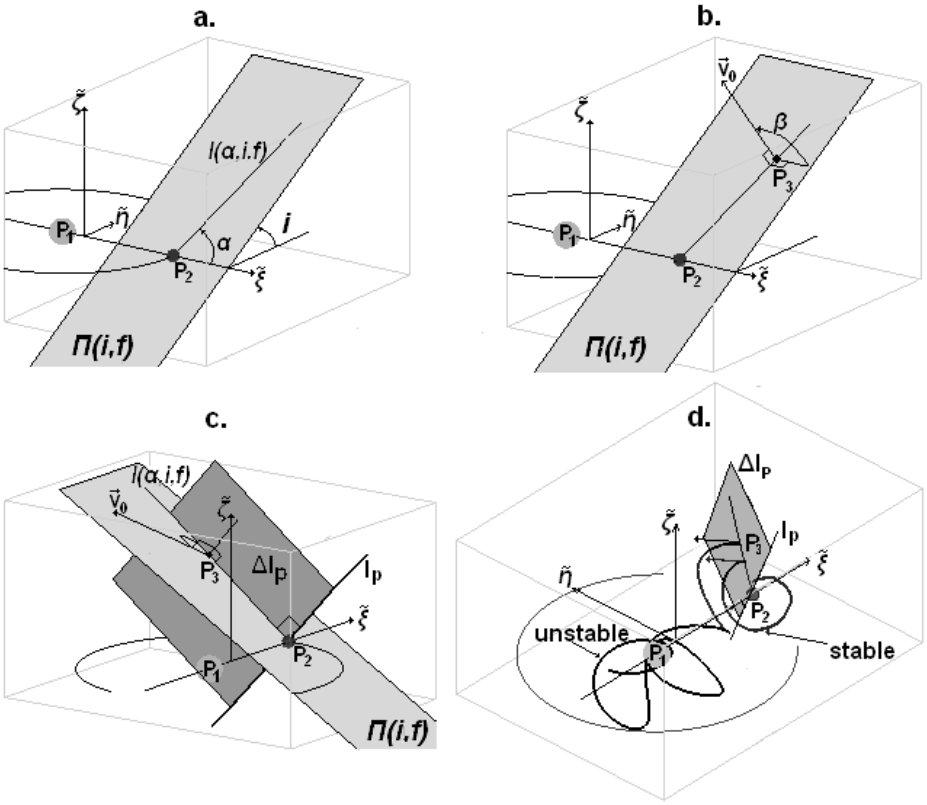


**Fig. 3** Stable and unstable trajectories relative to $P_2$

(iii) The initial velocity of the trajectory is perpendicular to the line $l(\alpha, i, f)$, making an angle $\beta$ with the plane $\Pi\,(i, f)$. The angle $\beta \in [0, 360^0)$ is measured in the counterclockwise direction if we look from $P_2$ towards $P_3$ (Figure 3.b). In this case the initial velocity relative to the $P_2$-centered reference frame is $v_0 = \sqrt{\frac{\mu(1+e_3)}{a_3(1-e_3)}}$. If $\beta = 180^0$ then $P_3$ lies at the periapsis of a prograde orbit, and if $\beta = 0^0$ then $P_3$ lies at the periapsis of a retrograde orbit.
The initial conditions of the trajectory with respect to the non-rotating system of coordinates $P_2xyz$ are:

$$
\begin{aligned}
x_0 &= r_0\left(\cos\alpha\cos f_0 - \sin\alpha\cos i\sin f_0\right), \\
y_0 &= r_0\left(\cos\alpha\sin f_0 + \sin\alpha\cos i\cos f_0\right), \\
z_0 &= r_0\sin\alpha\sin i, \\
\dot{x}_0 &= v_0\left(\cos\beta\sin\alpha\cos f_0 + \cos\beta\cos\alpha\cos i\sin f_0 + \sin\beta\sin i\sin f_0\right), \\
\dot{y}_0 &= v_0\left(\cos\beta\sin\alpha\sin f_0 - \cos\beta\cos\alpha\cos i\cos f_0 - \sin\beta\sin i\cos f_0\right), \\
\dot{z}_0 &= v_0\left(-\cos\beta\cos\alpha\sin i + \sin\beta\cos i\right).
\end{aligned}
\tag{13}
$$

To give the initial conditions of the corresponding flow under the dynamical system (2), we transform $(x_0, y_0, z_0, \dot{x}_0, \dot{y}_0, \dot{z}_0)$ into $(\tilde{\xi}_0, \tilde{\eta}_0, \tilde{\zeta}_0, \tilde{\xi}_0', \tilde{\eta}_0', \tilde{\zeta}_0')$ by using formulas

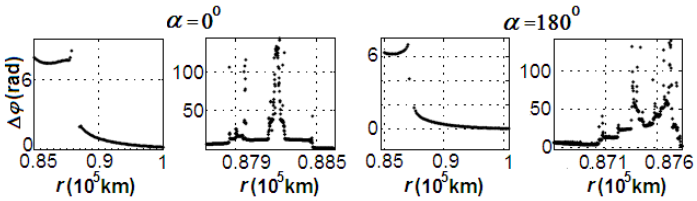


**Fig. 4** The variation of the capture effect $\Delta\varphi$ (expressed in radian) in the case of the Sun-Mercury system, with $i = 0^0$, $\beta = 180^0$ and $\alpha = 0^0$ (first and second picture) or $\alpha = 180^0$ (third and fourth picture). The second and fourth plot present details of the first and third plot around of the discontinuity points.

(7) and (9). For fixed values of the parameters $f, e_3, i, \beta$, and $\alpha$, the motion depends only on the distance $r_0$.

If the initial velocity lies in the plane $\Pi\,(i, f)$, i.e. $\beta \in \{0^0, 180^0\}$, to circumvent having multiple identical combinations of $i$ and $\beta$ (i.e. $(\beta = 0^0, i)$ represents the same case as $(\beta = 180^0, 180^0 - i)$ for all $i \in [0, 180^0]$), we introduce the auxiliary variable

$$I := \frac{i\beta}{180} + \frac{(180 - \beta)\,(180 - i)}{180}. \tag{14}$$

In this case, for prograde motions we have $\beta = 180^0$ and $i < 90^0$, or $\beta = 0^0$ and $i > 90^0$, and for retrograde ones $\beta = 180^0$ and $i > 90^0$, or $\beta = 0^0$ and $i < 90^0$. It is obvious that for $I < 90^0$ the motion is prograde, and for $I > 90^0$ the motion will be retrograde.

(iv) We consider the plane $\Delta$ normal to the initial velocity, and including the line $l(\alpha, i, f)$. Let $l_p$ be the line in $\Delta$ perpendicular to $l(\alpha, i, f)$ which contains $P_2$. We denote by $\Delta l_p$ the semi-plane of the $\Delta$, bounded by the line $l_p$ and including $P_3$, the initial position of the trajectory ($\Delta l_p$ marked dark gray in Figure 3.c).

(v) In our study the radius of the planet $P_2$ is considered to be $R_{P_2} > 0$. The motion and the corresponding initial state are said to be *stable* (identical to *1-stable*), if the massless particle $P_3$ leaving $l(\alpha, i, f)$ makes a complete turn around the planet $P_2$, without collision, and returns at a point of the semi-plane $\Delta l_p$ with negative Kepler energy relative to $P_2$, without making a complete turn around $P_1$ along his trajectory. This definition can be further generalized. It is possible to consider motions and their initial states which are $n$-stable ($n$ complete revolutions around $P_2$), introduced by García and Gómez in 2007. If the massless particle collides with the planet $P_2$ ($r_2 = R_{P_2}$) before it could make a complete turn around the planet $P_2$ with negative Kepler energy relative to $P_2$, then we have a *collisional motion* and its initial point is called a *collisional point*. In other cases, the motion and the corresponding initial state are said to be *unstable* (Figure 3.d).

(vi) The *weak stability boundary* (*WSB)* is the boundary of the regions of the stable points.

To investigate the return map to $\Delta l_p$ we can use the capture effect (Szenkovits et al. 2002). The *capture effect* $\triangle\varphi\,(x_0, y_0, z_0, \dot{x}_0, \dot{y}_0, \dot{z}_0)$ of the planet $P_2$ to the captured body $P_3$ with the initial conditions $(x_0, y_0, z_0, \dot{x}_0, \dot{y}_0, \dot{z}_0)$ and the flow $\gamma(f)$ is the total variation of the central angle $\triangle\varphi$ with respect to $P_2$ in the rotating frame during the capture, as long as $H_2\,(\gamma\,(f)) \leq 0$.

Performing numerical investigations concerning the capture effect in the Sun-Mercury system, in the framework of the ERTBP, we observe that:

(i) For fixed values of $f, e_3, i, \beta$ and $\alpha$ there exist $l_k^*$ $(k \geq 0)$ such that the variation of the capture effect depends smoothly on $r_0$ if $r_0 \in \left(l_{2k}^*, l_{2k+1}^*\right)$ and depends chaotic if $r_0 \in \left(l_{2k+1}^*, l_{2k+2}^*\right)$. Figure 4 shows this property applied to the Sun-Mercury system, where the orbital characteristics of Mercury are: $a = 46001210$ km, $e = 0.2053$, $\mu = 0.00000016601$. The chaotic behavior is in the discontinuity interval, where the capture effect changes its value from greater than $2\pi$ to less than $2\pi$.

(ii) If a point is stable, then the capture effect relative to this initial condition is greater than $2\pi$. Therefore, the WSB is a subset of the region where the capture effect changes its value from greater than $2\pi$ to less than $2\pi$, i.e. where the variation of the capture effect is chaotic (Figure 4).

The results presented above are in concordance with the results of García and Gómez (2007). The variation of the capture effect illustrates that the boundary between the stable and unstable regions has a chaotic structure.

## 3 Stable and unstable orbits in the Sun-Mercury system

First, we have investigated the structure of the weak stability region around the planet Mercury, when the inclination $i \in \left[0^0, 90^0\right]$ and the true anomaly $f_0 \in \left[0^0, 180^0\right]$ are variated. The value of the eccentricity $e_3 = 0$ is fixed. We consider the two cases when $P_3$ leaves the line $l(\alpha, i, f_0)$ in prograde direction ($\beta = 180^0$) or in retrograde direction ($\beta = 0^0$). In this study $\alpha$ varies between $0^0$ and $360^0$, and $r_0$ belongs to the $[R_M, 1.5R_H]$ interval, where $R_M = R_{P_2} = 2439.7$ km is the radius of planet Mercury and

$$R_H \approx a\,(1-e)\,\sqrt[3]{\frac{\mu}{3\,(1-\mu)}} = 139308km$$

is the radius of the Hill sphere (in this case the distance between $P_2$, the mass center of Mercury and $L_2$, the Lagrangian point between the Sun and Mercury).

By using numerical investigations we determined the stability, instability and collision regions, consisting of the initial positions corresponding to stable, unstable and collision orbits, for different values of the initial inclination $i \in \left[0, 90^0\right]$, with prograde ($\beta = 180^0$) and retrograde ($\beta = 0^0$) circular initial conditions ($e_3 = 0$). We have discretized the angular parameter $\alpha$ by using 360 equidistant values of $\left[0^0, 360^0\right)$ and the distance $r_0$ along $l(\alpha, i, f_0)$ with equidistant increments of 500 km between $R_M$ and $1.5R_H$. When we detected collision with Mercury, in fact crash on the surface of Mercury (i.e. $r_2 = R_M$, $R_M$ the radius of planet Mercury) we stopped the integration. In this way we avoided the necessity of using regularization, and we put in evidence an approximation of the real set of collisional orbits. Our set of collisional points contains all the initial positions corresponding to trajectories which pass through the singularity point where the center of the planet Mercury is located, but in addition, this set contains all the initial positions which lead to an impact with the surface of the planet Mercury. The results are presented in Figure 5, Figure 6 and Figure 7. The integration of the system (2) of the spatial ERTBP has been done by using a variable step size

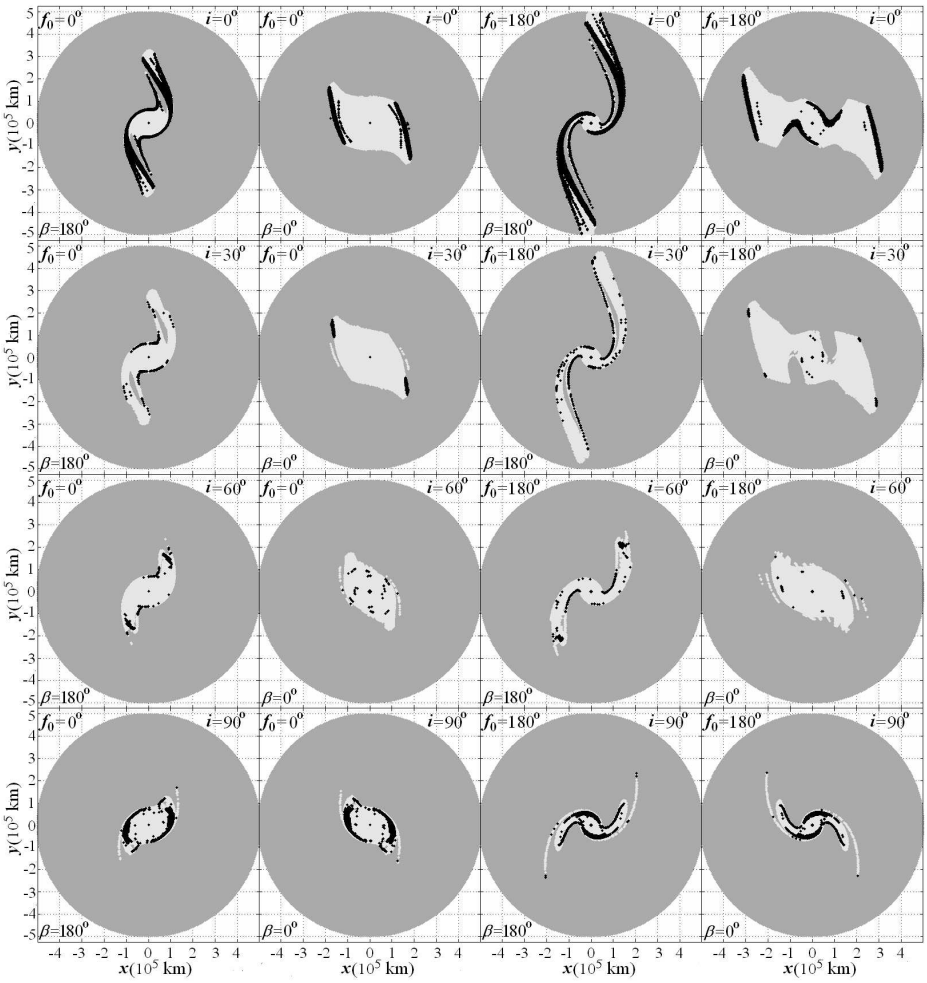


**Fig. 5** Stability regions for different values of the initial inclination and for initial true anomalies $f_0 \in \{0^0, 180^0\}$. The first and third columns state for the prograde (i.e. $\beta = 180^0$), the second and fourth columns for the retrograde motions (i.e. $\beta = 0^0$). The black points correspond to initial positions of collision orbits with planet Mercury, the dark gray points are initial positions of unstable motions, and the light gray points correspond to initial positions of stable motions.

Adams fourth-order predictor corrector scheme. The assumed local truncation error was less than $10^{-9}$.

In continuation of our study, we compared the stable and unstable regions for different values of the inclination $i$ and for the true anomaly $f_0 \in \left\{0^0, 180^0\right\}$. To perform this, we used the relative frequency of the stable, unstable, and collision points (i.e. the rate of number of the stable/unstable/collision points with respect to the total number of points) in the sections presented in Figure 5. The results are presented in Figure 8. Here we used the auxiliary variable $I$, given in (14), to illustrate the successive

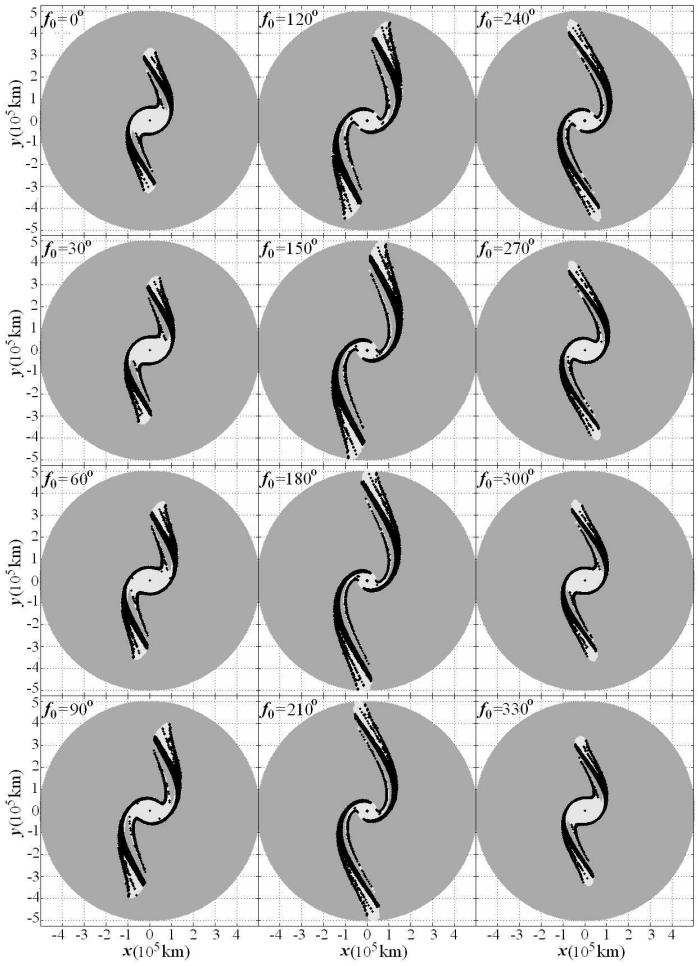


**Fig. 6** Stability regions for different values of the initial true anomaly, for prograde motions ($\beta = 180^0$ ) with an initial inclination of $i = 0^0$. The black points are initial positions of collision orbits with the planet Mercury, the dark gray points are initial positions of unstable motions, and the light gray points correspond to initial positions of stable motions.

extension of the variation of the relative frequencies related to the prograde ($I < 90^0$) and retrograde ($I > 90^0$) motions.

Investigating our results presented in Figure 5, Figure 6, Figure 7 and Figure 8 we can make some remarks.

(i) The relative frequency of the stable points is maximal when $I = 180^0$, i.e. when the motions are retrograde and the inclination $i = 0^0$(first picture of Figure 8).

(ii) Figure 6 and Figure 7 show that the stability regions change their shape and spread with respect to the variation of $f_0$. They expand when $f_0$ varies from $0^0$ to $180^0$, and then they contract when $f_0$ varies from $180^0$ to $360^0$. As we mentioned in the Section 1.1, the variation of the ZVS is correlated with the variation of the Hill stability $S(f)$. The measure of the Hill Stability $S(f)$ also increases when $f$ varies from $0^0$ to $180^0$ and then decreases as the spread of the stability regions

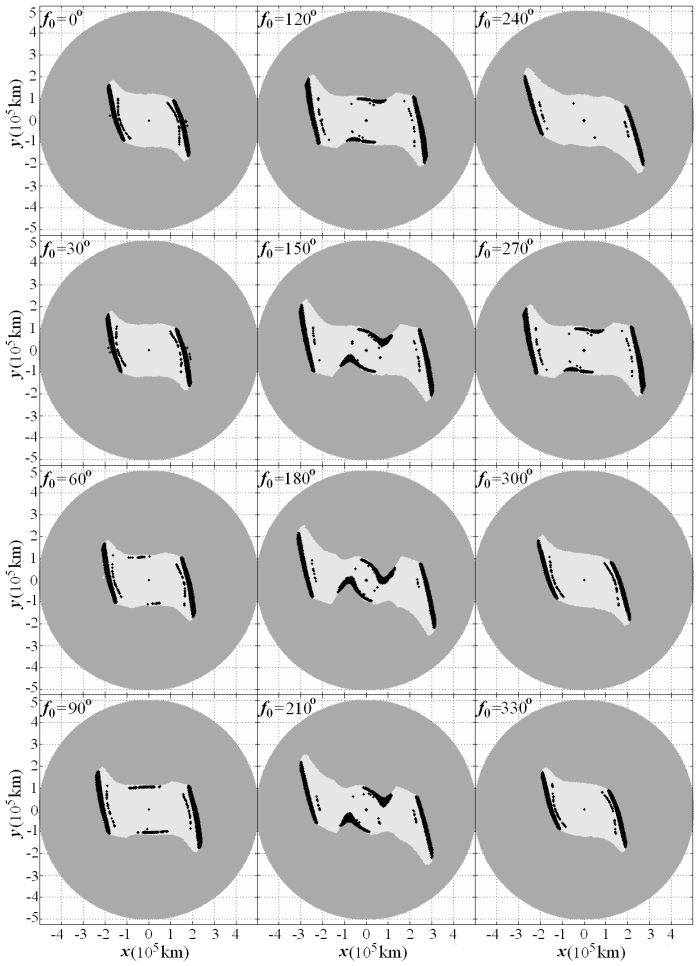


**Fig. 7** Stability regions for different values of the initial true anomaly, for an initial inclination of $i = 180^0$, in case of retrograde motions ($\beta = 0^0$). The black points are initial positions of collision orbits with the planet Mercury; the dark gray points are initial positions of unstable motions, and the light gray points correspond to initial positions of stable motions.

does. Therefore, the variation of the stability regions has the same rhythm as the pulsation of the ZVS (Figure 2). When the true anomaly $f$ increases from $0^0$ to $180^0$, then the distance $R = \|P_1P_2\|$ between the two primaries also increases, and then decreases when $f$ increases from $180^0$ to $360^0$ trough formula (1). This implies that the gravitational perturbing effect of $P_1$ to the initial states of $P_3$ around $P_2$ decreases. Accordingly, the stable regions are maximal for $f_0 = 180^0$ and minimal for $f_0 = 0^0$.

(iii) The collision regions are in the boundary of the stable regions, i.e. the collision regions are subsets of WSBs.

(iv) The relative frequency of the collision points is maximal in the case when the orbits are not inclined, i.e. $i = 0^0$, $\beta = 0^0$ or $\beta = 180^0$ (see the second picture of Figure 8).

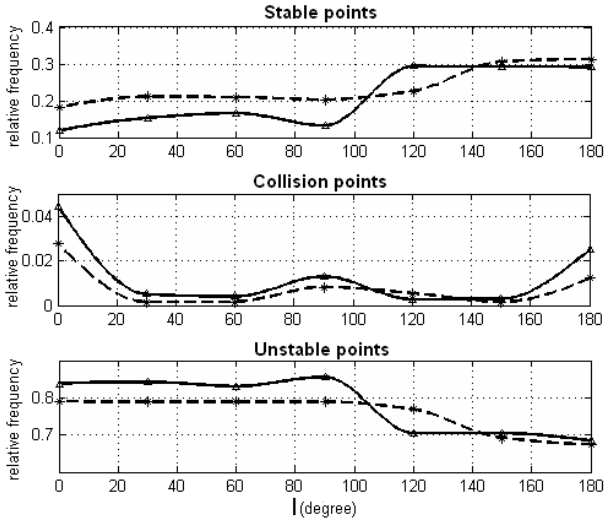


**Fig. 8** The variation of the relative frequency of stable, collision and unstable initial points with respect to the $I$ for $f_0 = 0^0$ (dashed line) and for $f_0 = 180^0$ (solid line), where $I := \frac{i\beta}{180} + \frac{(180-\beta)(180-i)}{180}$, $i \in \left[0^0, 90^0\right]$ and $\beta \in \left\{0^0, 180^0\right\}$.

(v) The crash orbits of the small body onto the primary $P_2$ are relatively frequent. This result is in concordance with the result obtained by Nagler in the framework of the planar CRTBP (Nagler 2005).
(vi) The stable regions present a central symmetry with respect to $P_2$. In the next we discuss this property in detail.

In the non-rotating system of coordinates $P_2xyz$ the initial conditions are given by the formula (13). We observe that for $\beta = 0^0$ or $\beta = 180^0$ these initial conditions are opposite for $\alpha$ and $\alpha + 180^0$. We use Monte Carlo simulations to investigate the following property: if an initial condition $(x, y, z, \dot{x}, \dot{y}, \dot{z})$ gives stable motion, then $(-x, -y, -z, -\dot{x}, -\dot{y}, -\dot{z})$ also gives stable motion.

We analyze this property for the fixed value of $e_3 = 0$ and $\beta = 0^0$, or $\beta = 180^0$. We use 100 000 initial positions with random values of $f_0 \in \left[0^0, 360^0\right)$, $\alpha \in \left[0^0, 360^0\right)$, $i \in \left[0^0, 90^0\right]$ and $r_0 \in [R_M, 1.5R_H]$. For each random vector $(f_0, \alpha, i, r_0)$ we construct two motions: the first one corresponding to the initial condition (13) with $\alpha$ and the second one with $\alpha + 180^0$. Then, we compare the stability types of these trajectories. We reached the conclusion that in the Sun-Mercury system the rate of coincidences for the stability region (the rate of symmetry of the stable region) is of 95% for prograde, and of 92% for retrograde motions.

## 4 Conclusions

The structure of the stable, unstable and collision regions around Mercury has been investigated by using the three-dimensional ERTBP model. For different values of the

initial inclination and initial true anomaly, numerical simulations proved that the relative frequency of the stable points increases with the inclination and is maximal when orbits are retrograde and not inclined. Figures 5, 6 and 7 illustrate that the boundaries of the stable regions also contain the initial points of collisional orbit to the planet Mercury. We can also deduce that the stable, unstable and collision regions pulsate with the revolution of the two primaries. This pulsation means that these regions slightly change their shape and spread with the variation of the true anomaly. This can be illustrated with short animations constructed by using the sections presented in Figure 6 or Figure 7. Finally, by using Monte Carlo simulations we put in evidence that the rate of symmetry of the stable regions for the Sun-Mercury system is of 95% for prograde, and 92% for retrograde motions.

**Acknowledgements** The authors express their gratitude for the useful recommendations of the unknown referees, which led to an essential improvement of this paper.

## References

1. E. Belbruno, Capture Dynamics and Chaotic Motions in Celestial Mechanics, Princeton University Press, 2004.
2. E. Belbruno, F. Topputo, M. Gidea, Resonance transitions associated to weak capture in the restricted three-body problem, Adv. Space Res., 42, 1330-1351 (2008).
3. E. Belbruno, J.K. Miler, Sun perturbed Eart-to-Moon transfers with Ballistic capture, J. Guid. Conrol. Dyn., 16, 770-775 (1993).
4. B. Érdi, E. Forgács-Dajka, I. Nagy, R. Rajnai, A parametric study of stability and resonances around $L_4$ in the elliptic restricted three-body problem, Celest. Mech. Dyn. Astron., 104, 145-158 (2009).
5. F. García, G. Gómez, A note on weak stability boundaries, Celest. Mech. Dyn. Astron., 97, 87-100 (2007).
6. R. Jehn, S. Campagnola, D. García, S. Kemble, Low-thrust approach and gravitational capture at Mercury, Proceedings of the 18th International Symposium on Space Flight Dynamics, 487-492 (2004).
7. R. Jehn, V. Companys, C. Corral, D. García Yárnoz, C. Sánchez, Navigaing BepiColombo during the weak-stability capture at Mercury, Adv. Space Res., 42, 1364-1369 (2008).
8. J. Nagler, Crash test for the restricted three-body problem, Phys. Rev. E 71, 026227(2005).
9. E. Perozzi , S. Ferraz-Mello (eds.), Space Manifold Dynamics, Springer, New York (2009).
10. D. Romagnoli, C. Circi, Earth-Moon weak stability boundaries in the restricted three and four body problem, Celest. Mech. Dyn. Astron., 103, 79-104 (2009).
11. V. Szebehely, Theory of orbits, Academic Press, New-York, 1967.
12. F. Szenkovits, Z. Makó, I. Csillik, A. Balint, Capture model in the restricted three-body problem, Pure Mathematics and Application, 13/4, 463-471 (2002).
13. F. Szenkovits, Z. Makó, About the Hill stability of extrasolar planets in stellar binary systems, Celest. Mech. Dyn. Astron., 101, 273-287 (2008).
14. F. Topputo, E. Belbruno, Computation of weak stability boundaries: Sun-Jupiter system, Celest. Mech. Dyn. Astron., 105, 3-17 (2009).
15. D.K. Yeomans, NASA jet propulsion laboratory: solar system dynamics, http://ssd.jpl.nasa.gov/ (2007).